


Cite this: *RSC Adv.*, 2020, 10, 39323



Received 1st September 2020

Accepted 19th October 2020

DOI: 10.1039/d0ra07509d

rsc.li/rsc-advances

# Confinement of a Au–N-heterocyclic carbene in a Pd<sub>6</sub>L<sub>12</sub> metal–organic cage†

Lihua Zeng,† Shujian Sun,‡ Zhang-Wen Wei,  Yu Xin, Liping Liu and Jianyong Zhang \*

A Au(I)–N-heterocyclic-carbene (NHC)-edged Pd<sub>6</sub>L<sub>12</sub> molecular metal–organic cage is assembled from a Au(I)–NHC-based bipyridyl bent ligand and Pd<sup>2+</sup>. The octahedral cage structure is unambiguously established by NMR, electrospray ionization-mass spectrometry and single crystal X-ray crystallography. The electrochemical behaviour was analyzed by cyclic voltammetry. The octahedral cage has a central cavity for guest binding, and is capable of encapsulating PF<sub>6</sub><sup>−</sup> and BF<sub>4</sub><sup>−</sup> anions within the cavity.

## Introduction

The self-assembly of metal–organic cages (MOCs)<sup>1–3</sup> has been investigated for diverse potential applications, such as catalysis,<sup>4</sup> sensing,<sup>5,6</sup> molecular storage and sequestration,<sup>7</sup> drug delivery,<sup>8</sup> and so on. For MOCs the shape, cavity size, and ligand can influence their guest binding and transformation capability.<sup>9–11</sup> N-heterocyclic-carbenes (NHCs) are a class of electron-donating ligands,<sup>12</sup> and have been applied in catalyzing various organic transformations.<sup>13,14</sup> Discrete assemblies based on NHC ligands including molecular metallocycles and cages have received increasing attention<sup>15–18</sup> because they may induce reactivity change, selectivity and product distribution variation.<sup>19,20</sup> However, few molecular cages with well-defined cavities are reported in the literature.<sup>21–23</sup> Remarkably, Nitschke *et al.* reported M<sub>4</sub>L<sub>6</sub> (M = Zn(II), Cd(II)) cages with Au(I)–NHC-based ligand.<sup>23</sup> In our effort to build NHC-based cages with large cavity, we wish to report herein that a Pd<sub>6</sub>L<sub>12</sub> metal–organic cage containing twelve Au(I)–NHC centres is assembled from a rigid, bent N-heterocyclic-carbene-based bipyridyl ligand and palladium(II) ions.

## Results and discussion

For the self-assembly of Pd<sub>6</sub>L<sub>12</sub> cage, bis(pyridyl)-functionalised Au(I)–NHC ligand **L** was designed and synthesized (Fig. 1a). First diiodo-functionalised imidazolium chloride (**b**) was synthesized from bis-Schiff's compound **a**<sup>24</sup> and para-formaldehyde *via* a ring-closing step in the presence of

chlorotrimethylsilane. Then Au(I)–NHC compound **c**<sup>25</sup> was synthesized by the reaction of imidazolium salt **b** with H<sub>2</sub>AuCl<sub>4</sub>·4H<sub>2</sub>O and 3-chloropyridine in the presence of base (Na<sub>2</sub>CO<sub>3</sub>). Subsequently, **L** was synthesized by Suzuki–Miyaura cross-coupling reaction between **c** and 3-pyridylboronic acid (Fig. S1–S10†). <sup>1</sup>H NMR shows that the imidazolium C–H resonance appeared at δ 10.34 for **b** and disappeared for **L**. <sup>13</sup>C NMR spectra show the resonance of the imidazolium C–H carbon at 139.60 ppm for **b** and the resonance of the metallated carbene-carbon atoms at 185.55 ppm. The coordination cage Pd<sub>6</sub>L<sub>12</sub> was successfully assembled by heating a 2 : 1 mixture of **L** and Pd(NO<sub>3</sub>)<sub>2</sub>·2H<sub>2</sub>O in DMSO at 70 °C for 6 h. <sup>1</sup>H NMR indicates that the quantitative formation of Pd<sub>6</sub>L<sub>12</sub> (12 NO<sub>3</sub><sup>−</sup> anions are omitted for clarity, the same hereinafter) (Fig. 2 and S11†). The cage is highly symmetric. Compared with the free ligand **L** the original sharp signals of pyridine moieties turn into broad peaks and shift downfield, for example the signals at 9.05, 8.64 and 8.26 ppm for the H<sub>i</sub>, H<sub>h</sub> and H<sub>c</sub> pyridyl protons are downfield-shifted to 9.74, 9.09 and 8.62 ppm, respectively, which is ascribed to the coordination of palladium(II) ions to the ligand.

Gratifyingly, single crystals of Pd<sub>6</sub>L<sub>12</sub> (NO<sub>3</sub><sup>−</sup> salt) suitable for X-ray diffraction analysis were obtained over one month by slow diffusion of ethyl acetate vapour into a solution of Pd<sub>6</sub>L<sub>12</sub> in DMSO (Table S1†). The crystals crystallize in the trigonal space group *R* $\bar{3}$ . The cubic symmetric unit is composed of six Pd(II) metal centres linked by twelve **L** ligands, forming the octahedron edges (Fig. 1b). Nevertheless, nitrate ions and solvent molecules could not be reasonably located in this highly disordered structure. The bend angle between pyridine rings and central Au–NHC ring is 174.1°. Two pyridyl donors on the same ligands adopt *syn*-conformation. The bond angles C<sub>carbene</sub>–Au–I<sub>trans</sub> range from 176 to 179° are in fact close to linearity (C18–Au1–I1 176.1(11)°) and the Au1–C18 bond length of 1.96(3) Å, which is close to those of the reported (NHC)gold(I) complexes.<sup>26</sup> Each Pd(II) has a square planar geometry with Pd–

MOE Laboratory of Polymeric Composite and Functional Materials, School of Materials Science and Engineering, School of Chemistry, Sun Yat-Sen University, Guangzhou 510275, China. E-mail: zhijyong@mail.sysu.edu.cn

† Electronic supplementary information (ESI) available: Additional experimental details, spectra and structure data. CCDC 2013514. For ESI and crystallographic data in CIF or other electronic format see DOI: 10.1039/d0ra07509d

‡ These authors contributed equally to the work.



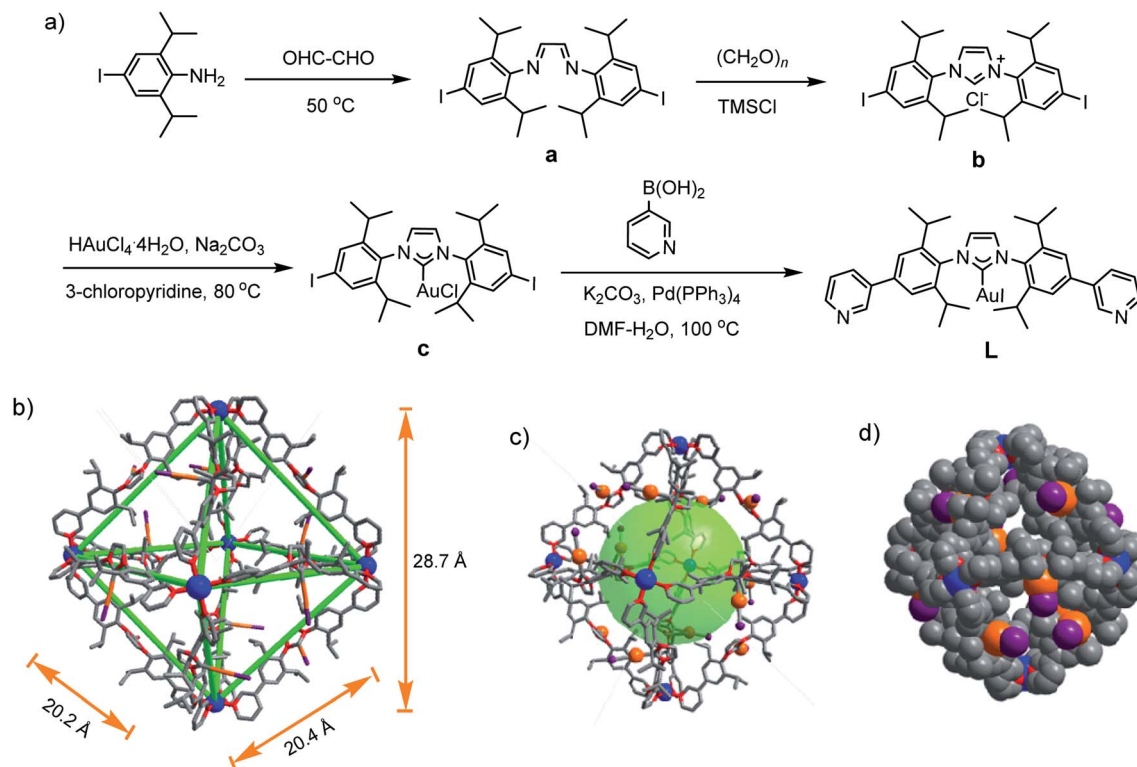


Fig. 1 (a) Synthetic route of **L**, single crystal X-ray structures of  $\text{Pd}_6\text{L}_{12}$ , (b) sticks, (c) ball-and-stick model, (d) space-filling model. Anions, solvent molecules and hydrogen atoms are omitted for clarity. Color coding: C: gray; N: red; I: purple; Au: orange; Pd: blue.

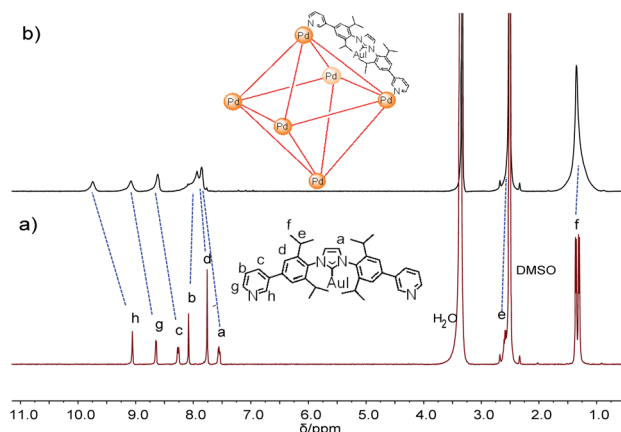


Fig. 2  $^1\text{H}$  NMR spectra of (a) **L** and (b)  $\text{Pd}_6\text{L}_{12}$  in  $\text{DMSO-}d_6$  (400 MHz, 298 K).

N bond distances of 1.98(2)–2.03(2) Å and the angle between the two 3-pyridyl coordinating motifs in **L** is  $88\text{--}93^\circ$ , within the normal range for those reported analogous pyridine-based ligand assembled  $\text{Pd}_6\text{L}_{12}$  complexes.<sup>27,28</sup> The cavity size is approximately  $20.2 \times 20.4 \times 28.7 \text{ \AA}^3$ , which is defined by the six Pd(II) ions. The opposing Pd(II)–Pd(II) distance is 28.7 Å and adjacent Pd–Pd distances are 20.2–20.4 Å. One of the two diisopropyl groups on each ligand points to the cavity, and the C–C distance of diisopropyl groups on opposite ligands is 16.3 Å.

Further evidence for  $\text{Pd}_6\text{L}_{12}$  was provided by  $^1\text{H}$ – $^1\text{H}$  homo-nuclear correlation spectroscopy (COSY) and  $^1\text{H}$ – $^1\text{H}$  nuclear overhauser effect spectroscopy (NOESY), which both reveal important cross peaks between the two observed sets of NMR signals (e.g.  $\text{H}_c$ – $\text{H}_b$  and  $\text{H}_c$ – $\text{H}_h$ ) (Fig. S12 and S13†). In addition, diffusion-ordered NMR spectroscopy (DOSY) shows the selective formation of a single species (Fig. S14†). The same diffusion coefficient at  $D = 5.75 \times 10^{-11} \text{ m}^2 \text{ s}^{-1}$  corresponds to the dynamic radius of 19.0 Å according to the Stokes–Einstein equation.<sup>28</sup> Further structural evidence was given by electrospray ionization-mass spectrometry (ESI-MS) (Fig. 3). After anion exchange of  $\text{NO}_3^-$  for  $\text{PF}_6^-$  ions in DMSO solution, a series of prominent peaks with continuous charge states of  $[\text{M}(\text{PF}_6^-)_n]^{n+}$  ( $n = 4\text{--}8$ ) were detected for  $\text{Pd}_6\text{L}_{12}$ . The isotopic distribution patterns of each peak agreed well with the simulated patterns.

The chemical composition of **L** and  $\text{Pd}_6\text{L}_{12}$  were characterized by Fourier transform infrared spectroscopy (FT-IR) (Fig. S15†). The absorption of  $\text{Pd}_6\text{L}_{12}$  at  $1632 \text{ cm}^{-1}$  corresponding to the C=N in-ring stretching in the pyridine rings shifts to lower energy compare with **L** at  $1638 \text{ cm}^{-1}$ , which is attributed to the coordination of **L** to  $\text{Pd}^{2+}$  via the nitrogen atom. Both **L** and  $\text{Pd}_6\text{L}_{12}$  exhibit characteristic C–N<sub>carbene</sub> bands typically at 1467 and  $1443 \text{ cm}^{-1}$ .<sup>29</sup> The strong absorption band at approximately  $1384 \text{ cm}^{-1}$  is attributed to the  $\text{NO}_3^-$  ions for  $\text{Pd}_6\text{L}_{12}$ .

To investigate the electrochemical behaviour, cyclic voltammetry analyses were carried out in the potential range from  $-2.0$



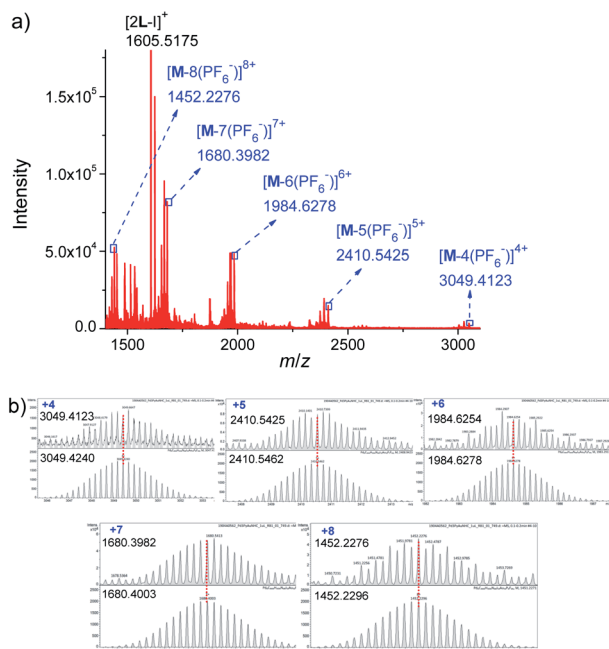


Fig. 3 (a) ESI-TOF-MS spectrum of  $\text{Pd}_6\text{L}_{12}$  (M) ( $\text{PF}_6^-$  as counterion) and (b) measured (top) and calculated (bottom) isotope patterns for various charge states observed for  $[\text{Pd}_6\text{L}_{12}]^{12+} \cdot 12\text{PF}_6^-$ .

to +2.0 V at a scan rate of  $50 \text{ mV s}^{-1}$  in a solution of tetrabutylammonium hexafluorophosphate ( $\text{TBAPF}_6$ ) in dry DMSO ( $0.10 \text{ mol L}^{-1}$ ) as a supporting electrolyte on glassy carbon electrode (3 mm in diameter) (Fig. 4). **L** gave a reduction wave at a potential of  $-1.068 \text{ V}$ , indicating the reduction of  $\text{Au}(\text{I})$  to metallic  $\text{Au}(0)$  corresponding to previously reported  $\text{Au}(\text{I})\text{-NHC}$  analogues.<sup>30,31</sup> The analogous process was significantly shifted to a more anodic potential at  $-0.890 \text{ V}$  for  $\text{Pd}_6\text{L}_{12}$ . In addition to the reduction processes, a single irreversible oxidation peak was also observed at  $0.812 \text{ V}$  for  $\text{Pd}_6\text{L}_{12}$ , positively shifted by  $0.287 \text{ V}$  from **L** ( $+0.525 \text{ V}$ ), which is consistent with the oxidation processes of  $\text{I}^-$  to  $\text{I}_2$  on clean glassy carbon surface.<sup>32,33</sup> It is worth noting that a new irreversible cathodic potential appeared at  $-0.732 \text{ V}$ , attributed to the reduction process of  $\text{NO}_3^-$  to  $\text{NO}_2^-$  within the cage,<sup>34</sup> perhaps owing to the change of ionic status in the cavity after coordination.<sup>35</sup> The reduction

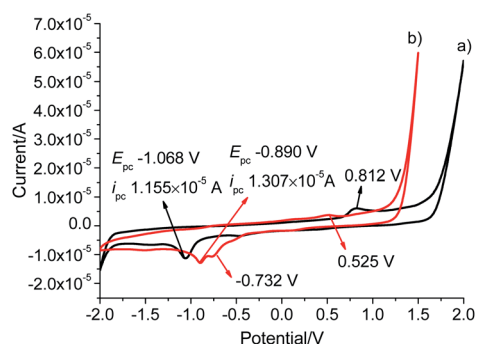


Fig. 4 Cyclic voltammograms of (a) **L** and (b)  $\text{Pd}_6\text{L}_{12}$  in DMSO solution at a scan rate of  $50 \text{ mV s}^{-1}$ , results are reported versus Ag wire.

current for  $\text{Pd}_6\text{L}_{12}$  were acquired at scan rates of  $50\text{--}200 \text{ mV s}^{-1}$ , showing that two reduction waves are located below the scan rates of  $100 \text{ mV s}^{-1}$  (Fig. S16†). With the increase in the sweep rate, the two waves merge into one broad peak, suggesting that the redox process takes place under simple diffusion-control for the cage.<sup>36</sup>

The resulting cage structure of  $\text{Pd}_6\text{L}_{12}$  was further investigated to explore its encapsulation of anions. The original nitrate anions are difficult to detect by NMR, so anion exchange of nitrate with other anions were performed. Various anions (20 equiv., excess) were added to a DMSO solution of  $\text{Pd}_6\text{L}_{12}$  ( $0.75 \text{ mmol L}^{-1}$ ) and the mixture was allowed to react for 4 h at room temperature, then diethyl ether was added to precipitate out pale yellow solid prior to the acquisition of NMR spectroscopy. After the introduction of  $\text{NaPF}_6$   $^{31}\text{P}$  NMR spectroscopy shows that phosphorus resonances from  $\text{PF}_6^-$  in DMSO appear expected sharp septet, with the main peak at  $\delta -144.19 \text{ ppm}$  with coupling constant of  $J_{\text{PF}} = 711.2 \text{ Hz}$ ,<sup>37</sup> while bound  $\text{PF}_6^-$  anions display the multiplets centred on  $\delta -142.70 \text{ ppm}$ , shifted by  $\Delta\delta = 1.49 \text{ ppm}$  with  $J_{\text{PF}} = 719.3 \text{ Hz}$  to lower field (Fig. 5a and S17†). Moreover,  $^{19}\text{F}$  NMR shows that one new set of peaks at  $-65.19 \text{ ppm}$  ( $J_{\text{FP}} = 725.7 \text{ Hz}$ ) are downshifted with free  $\text{PF}_6^-$  ( $-70.15 \text{ ppm}$ ,  $J_{\text{FP}} = 710.6 \text{ Hz}$ ) (Fig. 5b and S18†). Additionally for  $^1\text{H}$  NMR  $\text{H}_i$  proton resonance inside the central cavity is upfield shifted by  $0.70 \text{ ppm}$  (Fig. S19†), while other proton resonances are essentially unaffected. These results demonstrate that two types of  $\text{PF}_6^-$  anions are present in the solution, some are

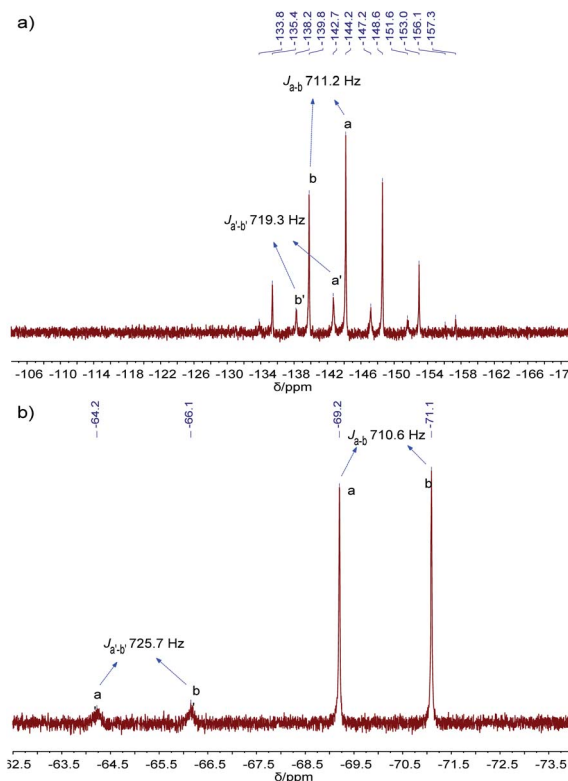


Fig. 5 (a)  $^{31}\text{P}$  NMR (162 MHz, 298 K), and (b)  $^{19}\text{F}$  NMR (376 MHz, 298 K) spectra of  $\text{PF}_6^- @ \text{Pd}_6\text{L}_{12}$  in  $\text{DMSO}-d_6$ .



encapsulated within the cavity, and others are free in the solution.

$\text{BF}_4^-$  anions can also be encapsulated inside the cavity. With the addition of  $\text{KBF}_4$  to  $\text{Pd}_6\text{L}_{12}$ ,  $^{19}\text{F}$  NMR shows two signals, one strong signal at  $-148.27$  ppm corresponding well with the peak of free  $\text{BF}_4^-$  in  $\text{DMSO}-d_6$  ( $-148.3$  ppm), and the other new signal at  $-144.1$  ppm (Fig. S20 and S21†).  $^{11}\text{B}$  NMR show that a new signal at  $2.79$  ppm is also assigned to bound  $\text{BF}_4^-$  in the cavity (Fig. S22 and S23†).<sup>38,39</sup> Simultaneously  $^1\text{H}$  NMR reveals that the proton resonance of  $\text{H}_i$  inside the central cavity is shifted upfield ( $\Delta\delta = 0.30$  ppm) compared to  $\text{Pd}_6\text{L}_{12}$  (Fig. S19†). These results suggest that some  $\text{BF}_4^-$  anions are bound within the cavity of  $\text{Pd}_6\text{L}_{12}$ . However, addition of  $\text{OTf}^-$  to  $\text{Pd}_6\text{L}_{12}$  causes neither new signals nor notable shifts, and  $^{19}\text{F}$  NMR gives only one sharp signal corresponding to free  $\text{OTf}^-$ , suggesting that the nitrate ions in the cage was unaffected by  $\text{OTf}^-$  (Fig. S19 and S24†).

## Conclusions

In summary, we have successfully synthesized  $\text{Au}(\text{I})$ -NHC bis-pyridine ligand (**L**) and  $\text{Au}(\text{I})$ -NHC-edged  $\text{Pd}_6\text{L}_{12}$  coordination cage has been assembled from **L** and  $\text{Pd}^{2+}$ . The cage  $\text{Pd}_6\text{L}_{12}$  has been fully characterized by NMR, diffusion-ordered NMR spectroscopy, FT-IR, mass spectrometry and cyclic voltammogram. The single crystal X-ray diffraction confirms unequivocally the octahedral structure of  $\text{Pd}_6\text{L}_{12}$ . The octahedral cage has central cavity for guest binding, and has been shown to be capable of encapsulating  $\text{PF}_6^-$  and  $\text{BF}_4^-$  anions within the cavity. It paves a way to build NHC-based metal-organic container molecules with large cavity for subsequent guest binding and transformation.

## Experimental

### Synthesis of **L**

A mixture of **c** (689.1 mg, 0.715 mmol), 3-pyridylboronic acid (357.5 mg, 2.86 mmol), anhydrous potassium carbonate (988.1 mg, 7.15 mmol), tetrakis(triphenylphosphine) palladium(0) (0.00715 mmol, 8.3 mg) in 18 mL degassed  $\text{DMF}-\text{H}_2\text{O}$  (v/v = 5 : 1) was stirred at  $100^\circ\text{C}$  for 24 h under argon atmosphere, the progress of the reaction was monitored by TLC. After completion of the reaction, the solvent was removed and the residue was dispersed in water and extracted with  $\text{CH}_2\text{Cl}_2$ . The  $\text{CH}_2\text{Cl}_2$  solution was washed with water and brine, dried over anhydrous  $\text{MgSO}_4$ , filtered and concentrated *in vacuo*. Purification by column chromatography on silica gel (ethyl acetate : hexane 1 : 1) to give the product as white powder which was further purified by washing with hexane (464 mg, 75%).  $^1\text{H}$  NMR (400 MHz,  $\text{DMSO}-d_6$ ):  $\delta$  9.05 (s, 2H), 8.64 (s, 2H), 8.27–8.22 (m, 2H), 8.08 (s, 2H), 7.76 (s, 4H), 7.57–7.53 (m, 2H), 2.59 (dt,  $J = 14.0, 6.9$  Hz, 4H), 1.36 (d,  $J = 6.8$  Hz, 12H), 1.30 (d,  $J = 6.9$  Hz, 12H).  $^{13}\text{C}$  NMR (101 MHz,  $\text{CDCl}_3$ ):  $\delta$  185.55, 149.02, 148.43, 146.49, 140.41, 136.25, 134.79, 133.79, 123.65, 123.29, 123.14, 29.04, 24.48, 24.06. Q-TOF-MS( $\text{ESI}^+$ ) ( $m/z$ ): calcd. for  $[\text{M} + \text{H}]^+$   $[\text{C}_{37}\text{H}_{43}\text{N}_4\text{Au}]^+$  867.2198, found 867.2206 and calcd. for  $[\text{M}-\text{AuI} + \text{H}]^+$   $[\text{C}_{41}\text{H}_{44}\text{N}_2\text{O}_2 + \text{H}]^+$  543.3488, found 543.3471.

### Synthesis of $\text{Pd}_6\text{L}_{12}$

**L** (174.0 mg, 0.2 mmol) and  $\text{Pd}(\text{NO}_3)_2 \cdot 2\text{H}_2\text{O}$  (27.0 mg, 0.1 mmol) were dissolved in  $\text{DMSO}$  (10.0 mL) were mixed. Each time 1 mL of the mixture was taken and stirred at  $70^\circ\text{C}$  for 6 h. The quantitative formation of  $\text{Pd}_6\text{L}_{12}$  was confirmed by  $^1\text{H}$  NMR and  $^1\text{H}$  DOSY NMR. The addition of diethyl ether to the yellow homogeneous solution precipitated the product, and it was collected by filtration, washed with diethyl ether, and dried *in vacuo* to give a pale yellow solid (13.8 mg, 70%).  $^1\text{H}$  NMR (500 MHz,  $\text{DMSO}-d_6$ ):  $\delta$  9.74 (s, 2H), 9.08 (s, 2H), 8.60 (s, 2H), 7.88 (d,  $J = 39.1$  Hz, 8H), 2.55 (s, 4H), 1.35 (s, 24H).  $^1\text{H}$  DOSY NMR (400 MHz,  $\text{DMSO}-d_6$ ):  $D = 7.16 \times 10^{-11} \text{ m}^2 \text{ s}^{-1}$ .  $\text{Pd}_6\text{L}_{12}(\text{PF}_6^- \text{ salt})$  was prepared by adding excess  $\text{NaPF}_6$  to the  $\text{DMSO}$  solution of  $\text{Pd}_6\text{L}_{12}$ . Electrospray ionization mass spectra were recorded for  $\text{Pd}_6\text{L}_{12}(\text{PF}_6^- \text{ salt})$ .  $m/z$  calcd for  $\text{C}_{444}\text{H}_{504}\text{N}_{48}\text{Au}_{12}\text{I}_{12}\text{P}_8\text{F}_{48}\text{Pd}_6$   $[\text{M}-4(\text{PF}_6)]^{4+}$  3049.4240, found 3049.4123;  $m/z$  calcd for  $\text{C}_{444}\text{H}_{504}\text{N}_{48}\text{Au}_{12}\text{I}_{12}\text{P}_7\text{F}_{42}\text{Pd}_6$   $[\text{M}-5(\text{PF}_6)]^{5+}$  2410.5462, found 2410.5425;  $m/z$  calcd for  $\text{C}_{444}\text{H}_{504}\text{N}_{48}\text{Au}_{12}\text{I}_{12}\text{P}_6\text{F}_{36}\text{Pd}_6$   $[\text{M}-6(\text{PF}_6)]^{6+}$  1984.6278, found 1984.6254;  $m/z$  calcd for  $\text{C}_{444}\text{H}_{504}\text{N}_{48}\text{Au}_{12}\text{I}_{12}\text{P}_5\text{F}_{30}\text{Pd}_6$   $[\text{M}-7(\text{PF}_6)]^{7+}$  1680.4003, found 1680.3982;  $m/z$  calcd for  $\text{C}_{444}\text{H}_{504}\text{N}_{48}\text{Au}_{12}\text{I}_{12}\text{P}_4\text{F}_{24}\text{Pd}_6$   $[\text{M}-8(\text{PF}_6)]^{8+}$  1452.2296, found 1452.2276;  $m/z$  calcd for  $\text{C}_{74}\text{H}_{84}\text{N}_8\text{Au}_2\text{I}$   $[\text{2L}-\text{I}]^+$  1605.5190, found 1605.5175.

### X-ray crystallography for $\text{Pd}_6\text{L}_{12}$

Quality single crystals were obtained by the slow diffusion of ethyl acetate vapour into a  $\text{DMSO}$  solution of  $\text{Pd}_6\text{L}_{12}$  ( $\text{NO}_3^-$  salt) to give colourless crystals of  $\text{Pd}_6\text{L}_{12}$  over one month. A crystal was picked ( $0.2 \times 0.2 \times 0.2 \text{ mm}^3$ ) and coated in paratone oil, attached to a glass silk which was inserted in a stainless steel stick, then quickly transferred to the Agilent Technologies SuperNova X-ray diffractometer with the Enhance X-ray Source of Cu  $\text{K}\alpha$  radiation ( $\lambda = 1.54184 \text{ \AA}$ ) using the  $\omega$ - $\phi$  scan technique. Data collection were measured at 150.00 (10) K. The unit cell parameters were solved by direct methods and the unit cell parameters refined against all data by anisotropic full-matrix least-squares methods on  $F^2$  with the SHELXL program.<sup>40</sup> Hydrogen atoms were calculated in ideal positions (riding model). All nitrate ions and solvent molecules could not be reasonably located because of highly disordered structures, and were removed by PLATON/SQUEEZE routine.<sup>41</sup>

Crystallographic data for  $\text{Pd}_6\text{L}_{12}$ :  $\text{C}_{74}\text{H}_{84}\text{Au}_2\text{I}_2\text{N}_8\text{Pd}$  FW = 1839.62, trigonal,  $R\bar{3}$ ,  $a = 29.8768$  (16)  $\text{\AA}$ ,  $b = 29.8768$  (16)  $\text{\AA}$ ,  $c = 74.341$  (3)  $\text{\AA}$ ,  $\alpha = 90^\circ$ ,  $\beta = 90^\circ$ ,  $\gamma = 120^\circ$ ,  $V = 57\,468$  (7)  $\text{\AA}^3$ ,  $Z = 18$ ,  $T = 150.00$  (10) K,  $\lambda = 1.54184 \text{ \AA}$ ,  $\rho_{\text{calcd}} = 0.957 \text{ mg m}^{-3}$ ,  $\mu = 9.349 \text{ mm}^{-1}$ , 13 205 reflections were collected (7693 were unique) for  $6.856 < 2\theta < 79.938$ ,  $R(\text{int}) = 0.0372$ ,  $R_1 = 0.0888$ ,  $wR_2 = 0.2668$  [ $I \geq 2\sigma(I)$ ],  $R_1 = 0.1033$ ,  $wR_2 = 0.2821$  (all data) for 725 parameters and 825 restraints, GOF = 1.059. Selected bond lengths and bond angles are presented in Table S1.† The crystal structure was submitted to the Cambridge Structural Database under the CCDC number 2013514.

## Conflicts of interest

There are no conflicts to declare.



## Acknowledgements

We gratefully acknowledge the NSF of Guangdong Province (2019A1515010710) for financial support.

## Notes and references

- M. M. J. Smulders, I. A. Riddell, C. Browne and J. R. Nitschke, *Chem. Soc. Rev.*, 2013, **42**, 1728–1754.
- M. Han, R. Michel, B. He, Y.-S. Chen, D. Stalke, M. John and G. H. Clever, *Angew. Chem.*, 2013, **125**, 1358–1362.
- O. Chepelin, J. Ujma, X. Wu, A. M. Z. Slawin, M. B. Pitak, S. J. Coles, J. Michel, A. C. Jones, P. E. Barran and P. J. Lusby, *J. Am. Chem. Soc.*, 2012, **134**, 19334–19337.
- C. J. Brown, F. D. Toste, R. G. Bergman and K. N. Raymond, *Chem. Rev.*, 2015, **115**, 3012–3035.
- D. P. August, G. S. Nichol and P. J. Lusby, *Angew. Chem., Int. Ed.*, 2016, **55**, 15022–15026.
- H. Lee, D. Kim, H. Oh and O.-S. Jung, *Chem. Commun.*, 2020, **56**, 2841–2844.
- M. B. Duriska, S. M. Neville, J. Lu, S. S. Iremonger, J. F. Boas, C. J. Kepert and S. R. Batten, *Angew. Chem., Int. Ed.*, 2009, **48**, 8919–8922.
- W. Cullen, S. Turega, C. A. Hunter and M. D. Ward, *Chem. Sci.*, 2015, **6**, 625–631.
- S. Löffler, J. Lübben, A. Wuttke, R. A. Mata, M. John, B. Dittrich and G. H. Clever, *Chem. Sci.*, 2016, **7**, 4676–4684.
- D. R. Martir, A. Pizzolante, D. Escudero, D. Jacquemin, S. L. Warriner and E. Zysman-Colman, *ACS Appl. Energy Mater.*, 2018, **1**, 2971–2978.
- Y. Li and A. H. Flood, *Angew. Chem., Int. Ed.*, 2008, **47**, 2649–2652.
- M. N. Hopkinson, C. Richter, M. Schedler and F. Glorius, *Nature*, 2014, **510**, 485–496.
- Z. Guo, N. R. Song, J. H. Moon, M. Kim, E. J. Jun, J. Choi, J. Y. Lee, C. W. Bielawski, J. L. Sessler and J. Yoon, *J. Am. Chem. Soc.*, 2012, **134**, 17846–17849.
- D. Zhang, H. Yang, A. Martinez, K. Jamieson, J.-P. Dutasta and G. Gao, *Chem.–Eur. J.*, 2014, **20**, 17161–17167.
- M.-M. Gan, J.-Q. Liu, L. Zhang, Y.-Y. Wang, F. E. Hahn and Y.-F. Han, *Chem. Rev.*, 2018, **118**, 9587–9641.
- C. Mejuto, G. Guisado-Barrios, D. Gusev and E. Peris, *Chem. Commun.*, 2015, **51**, 13914–13917.
- A. Rit, T. Pape and F. E. Hahn, *J. Am. Chem. Soc.*, 2010, **132**, 4572–4573.
- N. Sinha, F. Roelfes, A. Hepp, C. Mejuto, E. Peris and F. E. Hahn, *Organometallics*, 2014, **33**, 6898–6904.
- S. Roland, J. M. Suarez and M. Sollogoub, *Chem.–Eur. J.*, 2018, **24**, 12464–12473.
- A. C. H. Jans, X. Caumes and J. N. H. Reek, *ChemCatChem*, 2019, **11**, 287–297.
- P. J. Altmann and A. Pöthig, *Angew. Chem., Int. Ed.*, 2017, **56**, 15733–15736.
- G. Xu, S. Leloux, P. Zhang, J. M. Suárez, Y. Zhang, E. Derat, M. Ménand, O. Bistri-Aslanoff, S. Roland, T. Leyssens, O. Riant and M. Sollogoub, *Angew. Chem., Int. Ed.*, 2020, **59**, 7591–7597.
- W. J. Ramsay, J. A. Foster, K. L. Moore, T. K. Ronson, R. J. Mirgalet, D. A. Jefferson and J. R. Nitschke, *Chem. Sci.*, 2015, **6**, 7326–7331.
- H. Yang, G. Li, Z. Ma, J. Chao and Z. Guo, *J. Catal.*, 2010, **276**, 123–133.
- W. Wang, A. Zheng, P. Zhao, C. Xia and F. Li, *ACS Catal.*, 2014, **4**, 321–327.
- M. Pažický, A. Loos, M. J. Ferreira, D. Serra, N. Vinokurov, F. Rominger, C. Jäkel, A. S. K. Hashmi and M. Limbach, *Organometallics*, 2010, **29**, 4448–4458.
- K. Suzuki, M. Tominaga, M. Kawano and M. Fujita, *Chem. Commun.*, 2009, 1638–1640.
- C. Gütz, R. Hovorka, C. Klein, Q.-Q. Jiang, C. Bannwarth, M. Engeser, C. Schmuck, W. Assenmacher, W. Mader, F. Topić, K. Rissanen, S. Grimme and A. Lützen, *Angew. Chem., Int. Ed.*, 2014, **53**, 1693–1698.
- D. Rendón-Nava, D. Mendoza-Espinosa, G. E. Negrón-Silva, J. L. Téllez-Arreola, A. Martínez-Torres, A. Valdez-Calderón and S. González-Montiel, *New J. Chem.*, 2017, **41**, 2013–2019.
- L. Aldous, D. S. Silvester, C. Villagrán, W. R. Pitner, R. G. Compton, M. C. Lagunas and C. Hardacre, *New J. Chem.*, 2006, **30**, 1576–1583.
- F. J.-B. dit Dominique, H. Gornitzka, A. Sournia-Saquet and C. Hemmert, *Dalton Trans.*, 2009, 340–352.
- H. V. Huynh, S. Guo and W. Wu, *Organometallics*, 2013, **32**, 4591–4600.
- S. G. Bratsch, *J. Phys. Chem.*, 1989, **18**, 1–21.
- L. Szpyrkowicz, S. Daniele, M. Radaelli and S. Specchia, *Appl. Catal., B*, 2006, **66**, 40–50.
- F. Jiang, N. Wang, Z. Du, J. Wang, Z. Lan and R. Yang, *Chem.–Asian J.*, 2012, **7**, 2230–2234.
- T. S. Varley, M. Hirani, G. Harrison and K. B. Holt, *Faraday Discuss.*, 2014, **172**, 349–364.
- T. Endo, H. Murata, M. Imanari, N. Mizushima, H. Seki, S. Sen and K. Nishikawa, *J. Phys. Chem. B*, 2013, **117**, 326–332.
- B. E. Aroussi, L. Guénée, P. Pal and J. Hamacek, *Inorg. Chem.*, 2011, **50**, 8588–8597.
- M. D. Wise, J. J. Holstein, P. Pattison, C. Besnard, E. Solari, R. Scopelliti, G. Bricogne and K. Severin, *Chem. Sci.*, 2015, **6**, 1004–1010.
- G. Sheldrick, *Acta Crystallogr., Sect. A: Found. Crystallogr.*, 2008, **64**, 112–122.
- L. Spek, *Acta Crystallogr., Sect. C: Struct. Chem.*, 2015, **71**, 9–18.

